

# Treeing

Gregory L. Watson<sup>1\*</sup>, Michael Jerrett<sup>2</sup>, Colleen E. Reid<sup>3</sup> and Donatello Telesca<sup>1</sup>

<sup>1</sup> Department of Biostatistics, University of California, Los Angeles

<sup>2</sup> Department of Environmental Health Sciences, University of California, Los Angeles

<sup>3</sup> Geography Department, University of Colorado Boulder

October 5, 2021

## Abstract

Treeing combines the flexible mean structure of regression trees with the covariance-based prediction strategy of kriging into the base learner of an ensemble prediction algorithm. In so doing, it combines the strengths of the two primary types of spatial and space-time prediction models: (1) models with flexible mean structures (often machine learning algorithms) that assume independently distributed data, and (2) kriging or Gaussian Process (GP) prediction models with rich covariance structures but simple mean structures. We investigate the predictive accuracy of treeing across a thorough and widely varied battery of spatial and space-time simulation scenarios, comparing it to ordinary kriging, random forest and ensembles of ordinary kriging base learners. Treering performs well across the board, whereas kriging suffers when dependence is weak or in the presence of spurious covariates, and random forest suffers when the covariates are less informative. Treering also outperforms these competitors in predicting atmospheric pollutants (ozone and PM<sub>2.5</sub>) in several case studies. We examine sensitivity to tuning parameters (number of base learners and training data sampling proportion), finding they follow the familiar intuition of their random forest counterparts. We include a discussion of scalability, noting that any covariance approximation techniques that expedite kriging (GP) may be similarly applied to expedite treering.

*Keywords:* prediction, machine learning, space-time, spatial, regression trees, ensemble, Gaussian process

## 1 Introduction

Spatial or space-time prediction of a quantity based on observations of it at other locations or times (or both) is a common problem in fields as diverse as environmental health, real estate and mining.

---

\*gwatson@ucla.edu

Formally, the problem is to predict the value of a random field  $Y(d)$  at a new spatial or space-time location  $d_0 \in \mathcal{D}$  given  $n$  observations of the field at other locations,  $\mathbf{y}(\mathbf{d}) = [y_1(d_1), \dots, y_n(d_n)]'$ , where  $d$  is the spatial ( $\mathcal{D} \subset \mathcal{R}^2$ ) or space-time ( $\mathcal{D} \subset \mathcal{R}^3$ ) coordinates that index the field. Ancillary information in the form of covariates  $\mathbf{X}(d) = [X_1(d), \dots, X_p(d)]$  is generally available, in which case the goal is to predict  $Y(d_0) \mid \mathbf{X}(d_0), \mathbf{z}(\mathbf{d})$ , where  $\mathbf{z}(\mathbf{d}) = \{\mathbf{y}(\mathbf{d}), \mathbf{X}(\mathbf{d})\}$  is the observed data. The conditional expectation  $E[Y(d_0) \mid \mathbf{X}(d_0), \mathbf{z}(\mathbf{d})]$  is the usual predictive target, because it is the minimal mean squared error (MSE) prediction of  $Y(d_0) \mid \mathbf{X}(d_0), \mathbf{z}(\mathbf{d})$ .

If we suppose  $Y(d) \mid \mathbf{X}(d)$  is composed of a mean function  $f$  of the covariates at  $d$  plus an error  $\epsilon(d)$  that is independent of  $\mathbf{X}(d)$  and has expectation 0, i.e.,  $E[\epsilon(d)] = 0$ , then

$$Y(d) \mid \mathbf{X}(d) = f[\mathbf{X}(d)] + \epsilon(d). \quad (1)$$

The second moment of  $\epsilon(d)$  encodes the spatial or space-time dependence between values of the random field. In particular, let  $\Sigma[d_1, d_2] := \text{Cov}[\epsilon(d_1), \epsilon(d_2)]$ , where  $\Sigma$  is a positive semidefinite function defining the covariance between  $\epsilon(d_1)$  and  $\epsilon(d_2)$  (and therefore between  $Y(d_1)$  and  $Y(d_2)$ ) for any  $d_1, d_2 \in \mathcal{D}$ . In this setting, the conditional predictive target is decomposed as the sum of the mean function and the expected conditional error,

$$E[Y(d_0) \mid \mathbf{X}(d_0), \mathbf{z}(\mathbf{d})] = f[\mathbf{X}(d_0)] + E[\epsilon(d_0) \mid \mathbf{z}(\mathbf{d})]. \quad (2)$$

It will be useful to characterize alternative prediction techniques based on the assumptions they make regarding these two terms.

The dominant traditional approaches to spatial and space-time prediction, especially for interpolation, use simple mean structures to model  $f$  and rely primarily on exploiting the spatial or space-time dependence of the random field for prediction. The mean function is usually assumed to be linear in the covariates, i.e.,  $f[\mathbf{X}(d_0)] = \mathbf{X}(d_0)' \boldsymbol{\beta}$ , where  $\boldsymbol{\beta} \in \mathcal{R}^p$ .

There is a rich literature on covariance estimation in this context, ranging from simple parametric functions of the distance between points (Cressie, 2015; Gelfand et al., 2010) to sophisticated anisotropic functions (Paciorek and Schervish, 2006; Sang and Huang, 2012). Given an estimate of the covariance function,  $\hat{\Sigma}$ , prediction proceeds by computing the best linear unbiased predictor (BLUP),

$$\hat{Y}(d_0) \mid \mathbf{X}(d_0), \mathbf{z}(\mathbf{d}) = \mathbf{X}(d_0)' \hat{\boldsymbol{\beta}} + \hat{\Sigma}_0 \hat{\Sigma}(\mathbf{d})^{-1} [\mathbf{y}(\mathbf{d}) - \mathbf{X}(\mathbf{d}) \hat{\boldsymbol{\beta}}], \quad (3)$$

where  $\hat{\Sigma} := \hat{\Sigma}(\mathbf{d}, \mathbf{d})$  is the  $n \times n$  estimated covariance matrix of the observed data,  $\hat{\Sigma}_0 := \hat{\Sigma}(d_0, \mathbf{d})$  is the estimated covariance of the prediction location with the locations of the observed data, and  $\hat{\beta} = [\mathbf{X}(\mathbf{d})' \hat{\Sigma}(\mathbf{d})^{-1} \mathbf{X}(\mathbf{d})]^{-1} \mathbf{X}(\mathbf{d})' \hat{\Sigma}(\mathbf{d})^{-1} \mathbf{y}(\mathbf{d})$ . This prediction procedure is widely known as kriging after Danie Krige (Krige, 1951), the mining engineer who proposed it, and is a special case of the BLUP for generalized least squares (Goldberger, 1962). It is also the maximum a posteriori (MAP) prediction of  $Y(d_0)$  of a Bayesian Gaussian process (GP) model with an uninformative prior on  $\beta$  and an equivalent covariance structure. The common types of kriging in the literature (ordinary, universal, with external drift, etc.) amount to differences in which if any covariates are included in  $\mathbf{X}(d)$ . We remain general in notation but primarily envision a universal kriging model with the coordinates and additional covariates in  $\mathbf{X}(d)$  (Cressie and Wikle, 2015; Gelfand et al., 2010).

While the dependence structure in equation 3 is potentially very flexible, the mean structure is quite rigid, and  $\mathbf{X}(d_0)' \hat{\beta}$  may be a very poor estimator of the true mean  $f[\mathbf{X}(d_0)]$ . In particular, assuming  $f$  is linear and additive in the covariates is dubious, and the lack of regularization promotes overfitting.

In stark contrast stand a bevy of machine learning algorithms with flexible mean structures that have become popular for spatial and space-time prediction (Watson et al., 2019; Xu et al., 2018; Reid et al., 2015). These models estimate  $f$  with a flexible, possibly nonparametric  $\tilde{f}$ , but usually assume that, observations of the random field are independent of each other conditional on the covariates, i.e., that  $\text{Var}[\epsilon(d_1), \epsilon(d_2)] := 0$  for  $d_1 \neq d_2$ . From this it immediately follows that the expected conditional error in equation 2,  $E[\epsilon(d_0) \mid \mathbf{z}(\mathbf{d})]$  must be 0, an obviously false assumption in many spatial or space-time contexts. So while  $\tilde{f}[\mathbf{X}(d_0)]$  may be flexible enough to approximate  $f[\mathbf{X}(d_0)]$ , it is a biased estimator of  $E[Y(d_0) \mid \mathbf{X}(d_0), \mathbf{z}(\mathbf{d})]$ . There are certain exceptions to this characterization in the literature, and we defer a discussion of their merits to section 7.

The linear mean structure often assumed in kriging (and many other GP-based procedures) and the working independence assumption often made by machine learning tools are simply not realistic. However, their complementary strengths suggest they might be combined into an algorithm with flexible mean *and* covariance structures. We take precisely this approach, enriching regression trees with a kriging covariance model, and then ensembling them into a new prediction algorithm

which we call *treeging*, a portmanteau of *tree* and *kriging*. Treeging is implemented in a freely available R package at <https://github.com/gregorywatson/treeging>.

The remainder of this manuscript proceeds as follows. In the next section, we present the treeging algorithm. In sections 3 and 4, we illustrate its use on spatial and space-time data respectively, including extensive simulations and case studies. Section 5 investigates how performance depends upon tuning parameters, and section 6 discusses treeging in the context of large data sets. Finally, we close with a discussion.

## 2 Treeging

### 2.1 Mean Structure

We define treeging as an ensemble of base learners named *treeges*, which are regression trees enriched with kriging. A regression tree is a heuristically defined model that recursively partitions the covariate space according to the values of covariates, modeling the conditional expectation of  $Y(d)$  given  $\mathbf{X}(d)$  as

$$E[Y(d)|\mathbf{X}(d)] = f[\mathbf{X}(d), \boldsymbol{\theta}] = \sum_{\ell=1}^L f_{\ell}[\mathbf{X}(d), \boldsymbol{\theta}_{\ell}] 1[\mathbf{X}(d) \in \mathcal{X}_{\ell}], \quad (4)$$

where  $\mathcal{X}_1, \dots, \mathcal{X}_L$  partition the covariate space, and  $f_{\ell}[\mathbf{X}(d), \boldsymbol{\theta}_{\ell}]$  gives the conditional expectation  $Y(d)|\mathbf{X}(d)$  for observations with covariates that are in  $\mathcal{X}_{\ell}$  (the  $\ell$ -th leaf). When a constant leaf model is employed, i.e., when  $f_{\ell}[\mathbf{X}(d), \boldsymbol{\theta}_{\ell}] = \theta_{\ell}$ , the regression tree corresponds to a linear model with an  $n \times L$  design matrix  $\mathbf{X}_{\tau}(\mathbf{d})$  with a column for each leaf in the tree. The elements of each row of  $\mathbf{X}_{\tau}(\mathbf{d})$  are 0 except for a 1 at the element corresponding to the leaf of the tree in which the covariates associated with that row reside, i.e.,  $[\mathbf{X}_{\tau}(\mathbf{d})]_{i\ell} = 1[\mathbf{X}(d_i) \in \mathcal{X}_{\ell}]$ . Substituting  $\mathbf{X}_{\tau}(d)$  for  $\mathbf{X}(\mathbf{d})$  in equation 3 provides an alternative BLUP,

$$\tilde{Y}(d_0)|\mathbf{X}_{\tau}(d_0), \mathbf{z}(\mathbf{d}) = \mathbf{X}_{\tau}(d_0)' \hat{\boldsymbol{\beta}}_{\tau} + \hat{\Sigma}_0 \hat{\Sigma}(\mathbf{d})^{-1} [\mathbf{y}(\mathbf{d}) - \mathbf{X}_{\tau}(\mathbf{d}) \hat{\boldsymbol{\beta}}_{\tau}]. \quad (5)$$

The superlative designation of the BLUP as *best* suggests uniqueness but obscures the fact that the BLUP is specific to the choice of mean and covariance functions. Selecting an alternate mean function in equation 5 thus provides an alternate BLUP.

Table 1: True and estimated mean and dependence structures for spatial or space-time prediction.

	Mean Structure	Dependence Term
Truth	$f[\mathbf{X}(d_0)]$	$E[\epsilon(d_0) \mid \mathbf{z}(\mathbf{d})]$
Kriging	$\mathbf{X}(d_0)' \hat{\boldsymbol{\beta}}$	$\hat{\Sigma}_0 \hat{\Sigma}(\mathbf{d})^{-1} [\mathbf{y}(\mathbf{d}) - \mathbf{X}(\mathbf{d}) \hat{\boldsymbol{\beta}}]$
1 Regression Tree	$\mathbf{X}_\tau(d_0)' \hat{\boldsymbol{\beta}}_\tau$	0
1 Treege	$\mathbf{X}_\tau(d_0)' \hat{\boldsymbol{\beta}}_\tau$	$\hat{\Sigma}_0 \hat{\Sigma}(\mathbf{d})^{-1} [\mathbf{y}(\mathbf{d}) - \mathbf{X}_\tau(\mathbf{d}) \hat{\boldsymbol{\beta}}_\tau]$
Random Forest	$\frac{1}{B} \sum_{b=1}^B \mathbf{X}_\tau^{(b)}(d_0)' \hat{\boldsymbol{\beta}}_\tau^{(b)}$	0
Treeging	$\frac{1}{T} \sum_{t=1}^T \mathbf{X}_\tau^{(t)}(d_0)' \hat{\boldsymbol{\beta}}_\tau^{(t)}$	$\frac{1}{T} \sum_{t=1}^T \hat{\Sigma}_0^{(t)} \hat{\Sigma}(\mathbf{d}^{(t)})^{-1} [\mathbf{y}(\mathbf{d}^{(t)}) - \mathbf{X}_\tau^{(t)}(\mathbf{d}^{(t)}) \hat{\boldsymbol{\beta}}_\tau^{(t)}]$

Like regression trees, treeges exhibit low bias and high variance in their predictions on account of their tendency to overfit. Random forest improves upon the predictive performance of a single tree by combining many in an ensemble using bootstrap samples and random subsets of the covariates to reduce the variance of the predictions (Breiman, 2001). Motivated by this straightforward yet highly effective strategy, we ensembled treeges by training each one on a random subset of the training data, combining their predictions via a simple average. Differently from the iid case, data is sampled without replacement. The size of the subsample is a parameter that can be tuned, and by default we set to be  $m = \lfloor 0.632n \rfloor$ , because this is approximately the expected proportion of observations that appear in a bootstrap sample of size  $n$  (Efron and Tibshirani, 1997). We also mimic random forest in considering a subset of the covariates at each split. The resulting treeging prediction for  $Y(d_0)$  is

$$\tilde{Y}(d_0) \mid \mathbf{X}(d_0), \mathbf{z}(\mathbf{d}) = \frac{1}{T} \sum_{t=1}^T \left\{ \mathbf{X}_\tau^{(t)}(d_0)' \hat{\boldsymbol{\beta}}_\tau^{(t)} + \hat{\Sigma}_0^{(t)} \hat{\Sigma}(\mathbf{d}^{(t)})^{-1} [\mathbf{y}(\mathbf{d}^{(t)}) - \mathbf{X}_\tau^{(t)}(\mathbf{d}^{(t)}) \hat{\boldsymbol{\beta}}_\tau^{(t)}] \right\}, \quad (6)$$

where  $t = 1, \dots, T$  indexes treeges, and a superscript  $(t)$  indicates the data subset, design matrix or estimate for the  $t$ -th treege.

Table 1 lists the mean and dependence structures for kriging, random forest, a single treege and treeging. The limitations of kriging and random forest are apparent as is the manner in which they have been combined into treeging.

## 2.2 Covariance Estimation

Because a treege uses the same covariance structure as kriging, it accommodates any covariance estimation procedure that works for kriging. This makes available the wide variety of covariance structures developed for kriging, including procedures that iteratively estimate the mean and covariance, and importantly allows for the incorporation, of domain specific knowledge (Stein, 2005; Lloyd, 2010; Boisvert et al., 2009). It is also possible to use different covariance function estimators for different treeges within a treeging ensemble. The default covariance estimation strategy used for the results in this manuscript employs spherical covariance functions. Briefly, for each treege we fit a spherical variogram function to the empirical variogram of the regression tree residuals to estimate the parameters of a spherical covariance function. For space-time data, we fit separable spherical covariance functions to the spatial and temporal distances. The details of these procedures may be found in the appendix. One convenient feature of the spherical covariance function is that covariance decreases to 0 at a finite distance unlike other common choices, such as the exponential function. This can be exploited for computational expediency as we discuss in section 6.

## 2.3 Treeging Algorithm

Algorithm 1 describes the treeging algorithm in pseudocode for predicting a vector of outcomes,  $\mathbf{y}(\mathbf{d}_0)$ . For each of the  $T$  treeges, a random subsample of size  $\lfloor np \rfloor$ ,  $p \in (0, 1)$ , of the observed data is used to train a regression tree. Using an optimization procedure, the parameters of a spherical semi-variogram,  $\boldsymbol{\varphi}$  are fit to the residuals of the regression tree,  $\mathbf{e}_\tau^{(t)}(\mathbf{d}^{(t)})$ , and their pairwise distances,  $h_{ij} = \|d_i^{(t)} - d_j^{(t)}\|$ , for  $i, j = \{1, \dots, \lfloor np \rfloor\}$ . The estimated spherical parameters  $\boldsymbol{\varphi}^{(t)}$  provide an estimate of the covariance function,  $\hat{\Sigma}^{(t)}$ . Using this covariance function and the regression tree design matrix  $\mathbf{X}^{(t)}(\mathbf{d})$ , the treege prediction can be computed according to equation 5. Averaging the predictions of the  $T$  treeges yields the treeging prediction,  $\tilde{\mathbf{y}}(\mathbf{d}_0)$ .

## 3 Spatial Treeging

We investigated the suitability of treeging for spatial interpolation by comparing it to random forest, kriging and a kriging ensemble in a series of simulations and two case studies. The kriging

---

**Algorithm 1** Treeding

---

```
1: procedure TREEGING( $\mathbf{z}(\mathbf{d})$ ,  $\mathbf{d}_0$ ,  $\mathbf{X}_0(\mathbf{d}_0)$ ,  $p$ ,  $T$ )
2:   for  $t \leftarrow 1$  to  $T$  do
3:      $\mathbf{z}(\mathbf{d}^{(t)}) \leftarrow$  A random subset of size  $\lfloor np \rfloor$  from  $\mathbf{z}(\mathbf{d})$ 
4:      $\{\mathbf{X}_\tau^{(t)}(d), \hat{\boldsymbol{\beta}}_\tau^{(t)}\} \leftarrow$  Train a regression tree on  $\mathbf{z}(\mathbf{d}^{(t)})$ 
5:      $\mathbf{e}_\tau^{(t)}(\mathbf{d}^{(t)}) \leftarrow \mathbf{y}(\mathbf{d}^{(t)}) - \mathbf{X}_\tau^{(t)}(\mathbf{d}^{(t)})' \hat{\boldsymbol{\beta}}_\tau^{(t)}$ 
6:      $\gamma^{(t)}(h; \boldsymbol{\varphi}^{(t)}) \leftarrow$  Fit a spherical semi-variogram to  $\mathbf{e}_\tau^{(t)}(\mathbf{d}^{(t)})$  and their pairwise distances
7:      $\hat{\Sigma}_{ij}^{(t)} \leftarrow \Sigma(d_i^{(t)}, d_j^{(t)}; \boldsymbol{\varphi}^{(t)})$ ,  $i, j = 1, \dots, \text{round}(np)$ 
8:      $\hat{\Sigma}_0^{(t)} \leftarrow \Sigma(\mathbf{d}_0, \mathbf{d}^{(t)}; \boldsymbol{\varphi}^{(t)})$ 
9:      $\tilde{\mathbf{y}}^{(t)}(\mathbf{d}_0) \leftarrow \mathbf{X}_\tau^{(t)}(\mathbf{d}_0) \hat{\boldsymbol{\beta}}_\tau^{(t)} + \hat{\Sigma}_0^{(t)} \hat{\Sigma}^{(t)-1} [\mathbf{y}(\mathbf{d}^{(t)}) - \mathbf{X}_\tau^{(t)}(\mathbf{d}^{(t)}) \hat{\boldsymbol{\beta}}_\tau^{(t)}]$ 
10:   end for
11:    $\tilde{\mathbf{y}}(\mathbf{d}_0) \leftarrow \frac{1}{T} \sum_{t=1}^T \tilde{\mathbf{y}}^{(t)}(\mathbf{d}_0)$ 
12: end procedure
```

---

ensemble is constructed using the same subsampling and ensembling procedures as treeding, but with a linear mean structure for the base learners rather than the tree-based mean structure of treeges. Kriging ensembles are not commonly used, however, we included it in the comparison to discern the predictive gains or losses associated with treeding's flexible mean structure from those of ensembling.

We used  $R^2$  as our primary measure of predictive accuracy, which is the ratio of the mean squared prediction error to the variance,

$$R^2(\mathbf{y}, \hat{\mathbf{y}}) = 1 - \frac{\sum_{i=1}^n (y_i - \hat{y}_i)^2}{\sum_{i=1}^n (y_i - \bar{y})^2}, \quad (7)$$

where  $\bar{y}$  is the mean of  $\mathbf{y}$ . This is often interpreted as the proportion of the variation in  $\mathbf{y}$  explained by predicted values  $\hat{\mathbf{y}}$ , but the  $R^2$  can be negative if it is a worse predictor than  $\bar{y}$ , which is quite possible in out-of-sample prediction in which case the sample mean is unknown. In the simulation setting, the true  $R^2$  can be computed. In the case studies, we estimate the  $R^2$  using 10-fold cross-validation (CV), denoting the estimate as  $\hat{R}_{CV}^2$ .

### 3.1 Spatial Simulation Study

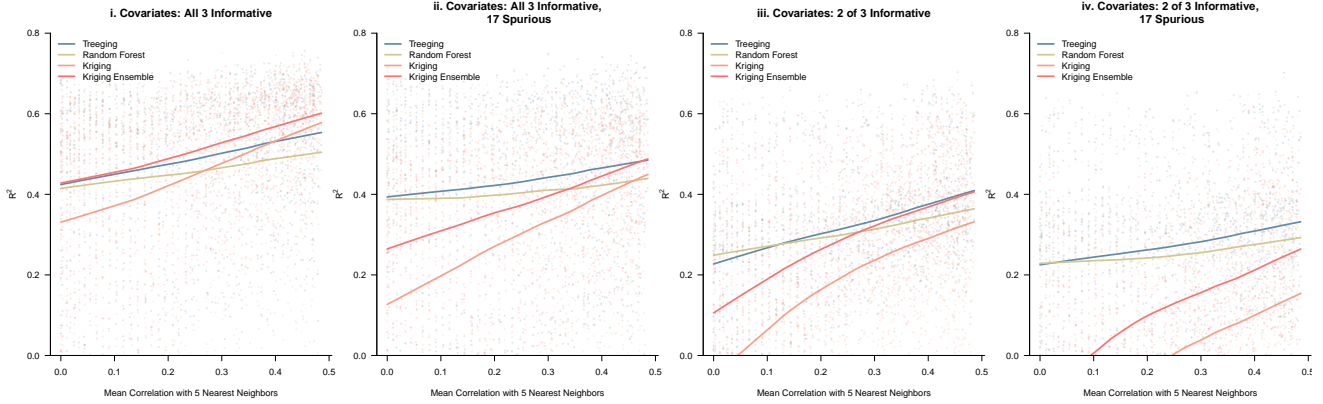
We simulated 1,029 spatial random fields across a variety of covariate effect sizes and levels of spatial dependence. In each case, the field was generated from a Gaussian process with a mean function depending on 3 covariates, one with a linear effect, one a threshold effect, and one a sigmoidal effect to mimic what is often encountered in environmental pollution studies. The mean function was scaled up or down using an effect size multiplier to elucidate the relationship between predictive performance and covariate effect size. The appendix provides the mean function and simulation parameters. We randomly selected 100 locations in a spatial domain as the observed data on which to train the models, and assessed their predictive accuracy over a  $21 \times 21$  grid of points across the spatial field under 4 different covariate scenarios: (i) the 3 informative covariates, (ii) the 3 informative covariates plus 17 spurious covariates, (iii) 2 of the 3 informative covariates selected at random, and (iv) 2 of the 3 informative covariates plus the 17 spurious covariates. In addition, the spatial coordinates were included as covariates in all cases. These 4 scenarios were constructed to reflect some of the common challenges encountered in spatially dependent data. Often there are potentially informative ancillary data, but which covariates are informative is unknown a priori, and not all relevant covariates may be available.

Figure 1A depicts the predictive  $R^2$  for each model under each covariate scenario as a function of the spatial dependence, which is assessed as the mean correlation between the prediction locations and the five nearest training data points. The results are smoothed using a LOWESS curve to facilitate comparison. Not surprisingly, there is a general increasing trend in  $R^2$  as spatial dependence increases for all models across every scenario, as increased spatial dependence corresponds to additional information with which to predict  $Y(d)$  over the unobserved grid. This increase is less pronounced for random forest, which ignores dependence, although it is able to make some gains, because the spatial coordinates are included as covariates.

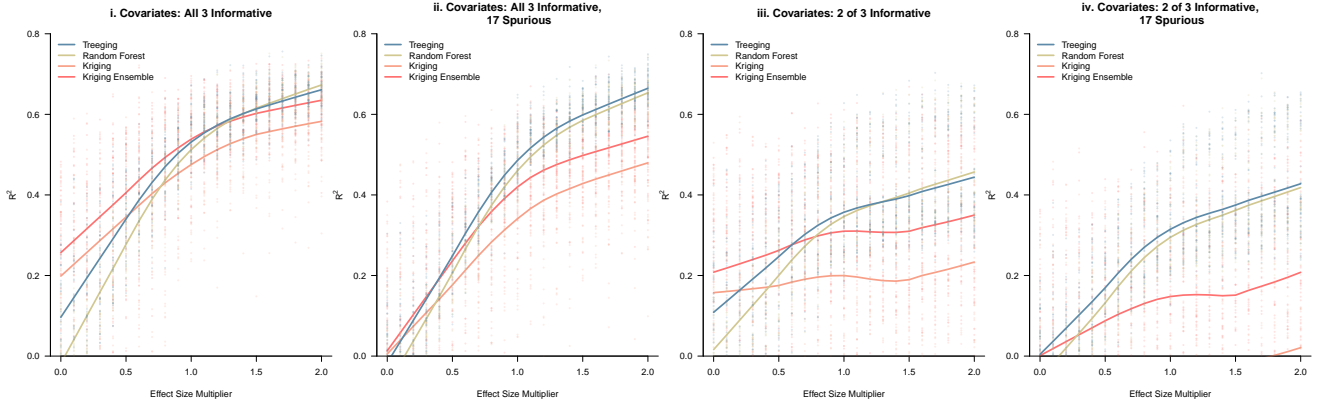
The kriging ensemble is the best performing model when trained on all three informative covariates without any spurious covariates (scenario i), with treering second best until it is overtaken by kriging at high levels of dependence. In the presence of spurious covariates (scenario ii), treering is the best model with the kriging ensemble performing comparably at high levels of dependence. In scenarios iii and iv, kriging and the kriging ensemble perform very poorly. Across all four scenarios, random forest performs respectably, but treering outperforms it across the board



## A. Predictive Accuracy as a Function of Spatial Dependence



## B. Predictive Accuracy as a Function of Covariate Effect Size



## C. Most Accurate Model as a Function of Spatial Dependence and Covariate Effect Size

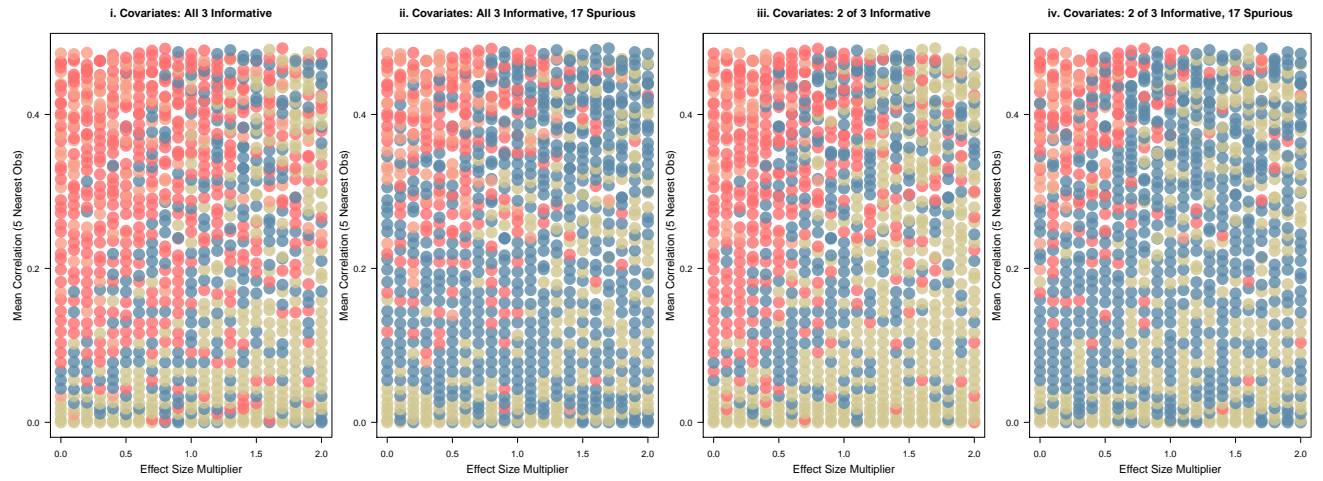


Figure 1: Spatial Simulation Model Comparison: Predictive accuracy ( $R^2$ ) as a function of (A.) spatial dependence, (B.) covariate effect size, and (C.) both. In (C.) the color of each dot depicts the highest  $R^2$  model for the simulation at that combination of the effect size multiplier and mean correlation.

with a small margin between them at low spatial correlation that increases as dependence gets stronger.

Figure 1B plots the marginal effect size multiplier against  $R^2$  for the same set of simulations. Across all four covariate scenarios there is again a consistent relationship between treeing and random forest. When the effect size multiplier is 0, the covariate effects are 0 and random forest performs poorly. Treeing performs noticeably better, although it is also not particularly accurate. As covariate effect strengths increase, the  $R^2$  for both treeing and random forest increases rapidly with random forest gradually closing the gap between them. Kriging and ensembled kriging perform fairly well when trained on all the informative covariates (scenarios i and ii) with the ensemble generally superior. At 0 effect size they have higher  $R^2$  than treeing and random forest, but are overtaken as effect size increases. In scenarios iii and iv, however, they perform very poorly with  $R^2$  decreasing as covariate effect size increases. Despite this additional predictive information, the mean structure of kriging is apparently too rigid when an informative covariate is withheld.

Figure 1C plots effect size against mean correlation with the color of each dot depicting the best (i.e., highest  $R^2$ ) model for that simulation. At low effect sizes (the left edge), kriging and ensembled kriging are generally best except when there is very little or no spatial dependence. When there is low dependence (the bottom edge), random forest and treeing are best. With the exception of scenario i, when there is substantial spatial dependence and effect size, treeing tends to be best.

## 3.2 Spatial Case Studies

We compared the predictive accuracy of the same set of models on daily 8-hour maximum average ozone and 24-hour average fine particulate matter ( $\text{PM}_{2.5}$ ) concentrations during wildfires in California in 2008 (Watson et al., 2019). Data were collected from 100 ozone and 45  $\text{PM}_{2.5}$  monitors over 118 and 120 days respectively. In addition to these data, 15 covariates including atmospheric weather data, land use information and chemical transport model predictions were collected along with the spatial coordinates. These covariates and their sources are listed in the appendix. To compare their accuracy at strictly spatial interpolation, we considered each day of the data as a distinct data set and estimated predictive accuracy using 10-fold CV, taking the average of each

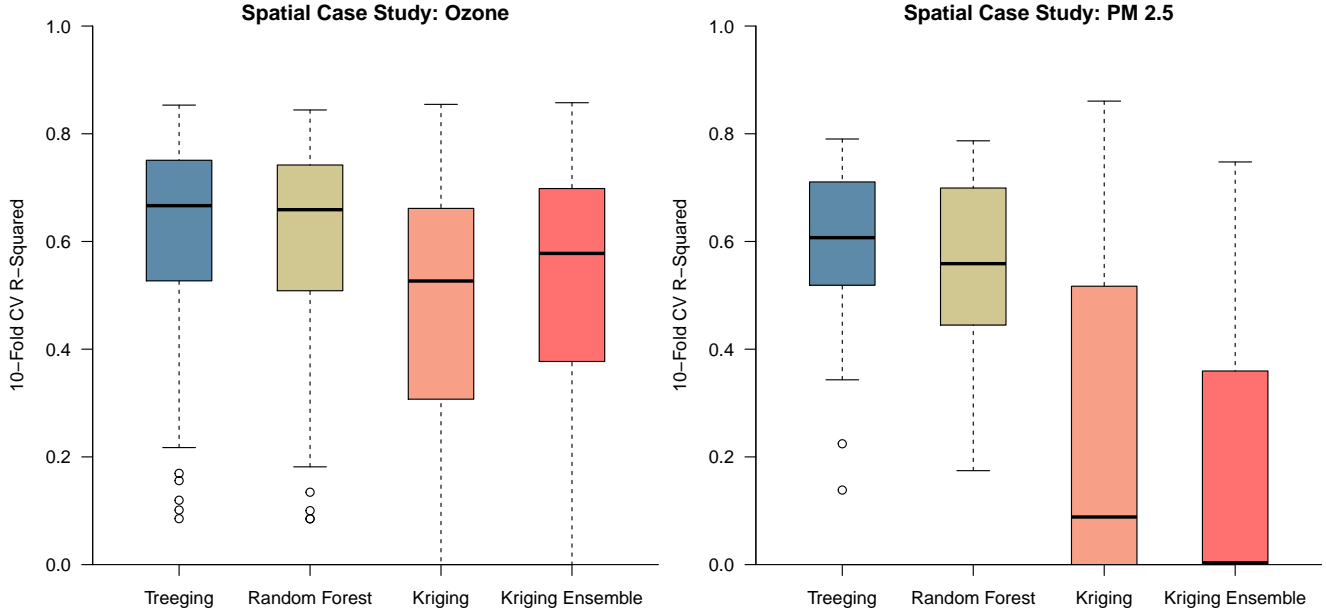


Figure 2: Spatial Case Studies Model Comparison: 10-fold CV estimates of  $R^2$  were produced for each day, treating each day as an independent spatial data set. The resulting distribution of estimates is summarized for each model as a boxplot, with the darkened central line indicating the median  $\hat{R}_{CV}^2$  across all days for that model.

day’s 10 folds as the estimated  $\hat{R}_{CV}^2$  for that day. In Section 4.2 we evaluate interpolation on the entire data set in our discussion of space-time treering, which is a more realistic approach to interpolation on these data.

Figure 2 depicts the average  $\hat{R}_{CV}^2$  on each day for each of the models on  $PM_{2.5}$  and ozone as box and whisker plots. For both pollutants, treering was the most accurate model (ozone  $\hat{R}_{CV}^2$ : 0.62,  $PM_{2.5}$   $\hat{R}_{CV}^2$ : 0.58), performing slightly better than random forest (ozone  $\hat{R}_{CV}^2$ : 0.61,  $PM_{2.5}$   $\hat{R}_{CV}^2$ : 0.56). For ozone, the kriging models are somewhat less accurate on average (kriging  $\hat{R}_{CV}^2$ : 0.43, ensemble  $\hat{R}_{CV}^2$ : 0.48), and worryingly have substantially higher variance. For  $PM_{2.5}$ , this variation is even greater, and the CV  $\hat{R}_{CV}^2$  is also much lower (kriging  $\hat{R}_{CV}^2$ : 0.00, ensemble  $\hat{R}_{CV}^2$ : -0.24). These results suggest that kriging models may be less stable than models with built-in feature selection like treering and random forest.

## 4 Space-Time Treeding

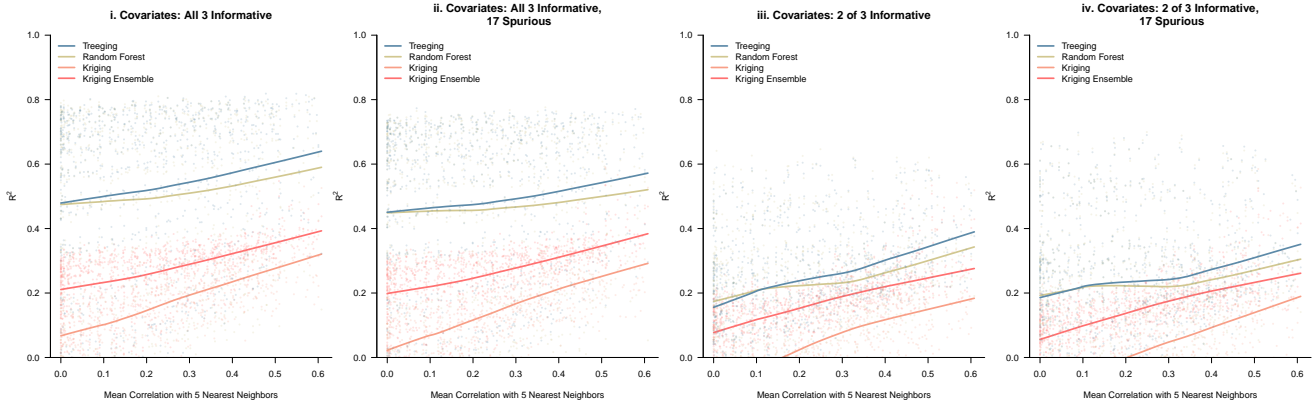
Space-time treeding considers prediction of a random field  $Y(d)$  indexed over a 3-dimensional space-time domain,  $\mathcal{D} \subset \mathcal{R}^3$ . In the context of space-time data, multiple types of prediction are possible (Watson et al., 2020b). We consider here the suitability of treeding for space-time interpolation, a common type of space-time prediction in which repeated measurements are taken at a set of locations and the predictive goal is to predict the entire time series at new spatial locations. This specific predictive target is motivated by typical applications in environmental pollution studies, which require the estimation of pollutant concentration as a potential source of exposure at unobserved spatial locations (Watson et al., 2020b).

### 4.1 Space-Time Simulation Study

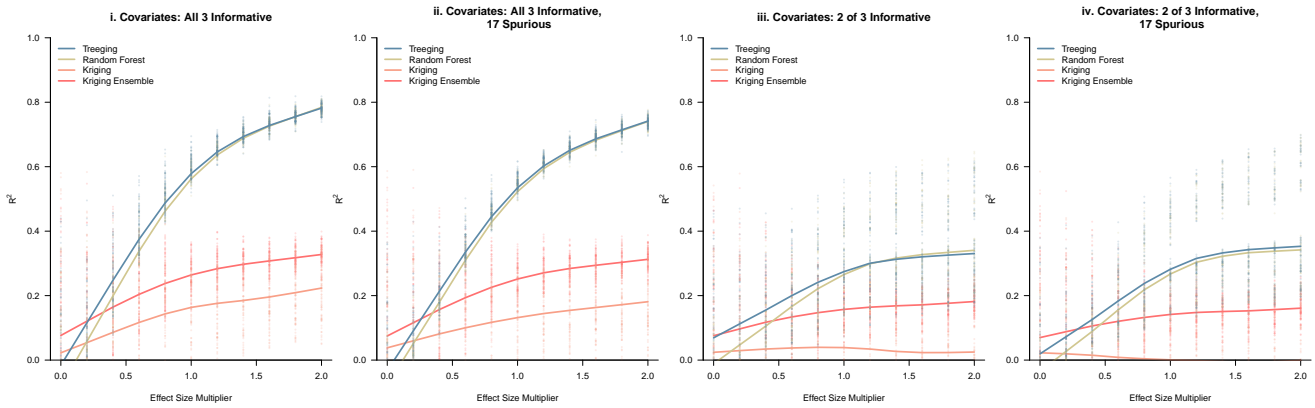
We conducted a second battery of simulations to investigate the predictive accuracy of space-time treeding. The random field  $Y(d)$  was sampled as a Gaussian process over a time series of length 30 at each of 40 training locations and an  $11 \times 11$  grid of test locations. The spatial dependence, temporal dependence and covariate effect sizes were varied to investigate their impact on predictive accuracy. The precise details and the functional forms of the covariates may be found in the appendix. Similarly to the spatial simulation study described above, we considered four covariate scenarios.

Figure 3 shows the results of the simulation study. Figure 3A depicts predictive  $R^2$  as a function of the mean correlation between test points and the five training points with which they are most highly correlated. The functional relationship between mean correlation and  $R^2$  is estimated using a LOWESS curve for each of the four models. In all four of the covariate scenarios, treeding (blue) and random forest (green) have nearly identical  $R^2$  when the mean correlation is 0, i.e., when there is no dependence, which is the left hand extreme of the plots. As the mean correlation increases, the  $R^2$  for random forest increases slightly, while that of treeding improves more rapidly, resulting in increasing divergence between these two curves. Treeding better exploits the additional information in the increasing dependence between training and test points, because it explicitly models this dependence, while random forest assumes there is none. Kriging (orange) and ensembled kriging (red) also improve as the mean correlation increases, since they too model the space-time dependence. Kriging is consistently below the kriging ensemble,

## A. Predictive Accuracy as a Function of Spatial Dependence



## B. Predictive Accuracy as a Function of Covariate Effect Size



## C. Most Accurate Model as a Function of Spatial Dependence and Covariate Effect Size

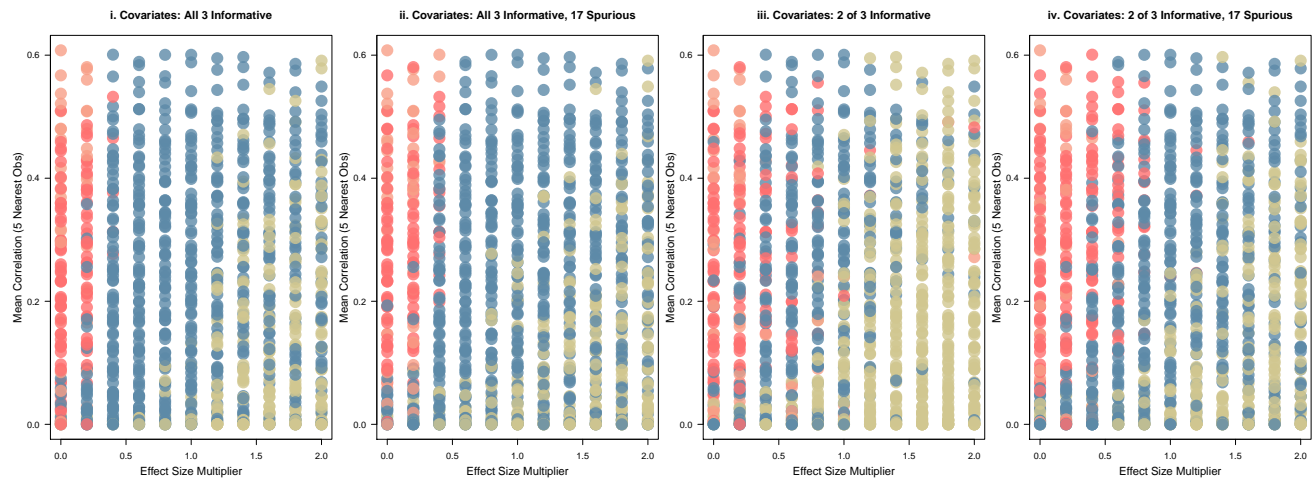


Figure 3: Space-Time Simulation Model Comparison: Predictive accuracy ( $R^2$ ) as a function of (A.) spatial dependence, (B.) covariate effect size, and (C.) both. In (C.) the color of each dot depicts the highest  $R^2$  model for the simulation at that combination of the effect size multiplier and mean correlation.

which is not surprising given the well known improvements in predictive accuracy associated with ensembling base learners.

Figure 3B depicts predictive  $R^2$  as a function of covariate effect size for the same set of simulations. Again kriging lags the kriging ensemble by a consistent amount. When the effect size multiplier is 0, the covariates have no effect on the outcome, aside from possible marginal associations with space or time resulting from the space-time dependence, random forest has the worst  $R^2$  in all four scenarios, because it relies exclusively on the relationship between the covariates and the outcome. Not surprisingly it is at this extreme that treeing excels random forest by the largest margin. It is also at this extreme that the kriging models tend to predict better than treeing. It would seem that treeing’s flexible mean structure hurts its accuracy in the absence of informative covariates, likely on account of the greater potential for overfitting. As the effect size multiplier increases, the covariates exert a stronger effect, treeing and random forest surpass the kriging models on the strength of their flexible mean structures, and random forest gradually closes the gap with treeing as the information in the covariates dominates that of the space-time dependence.

Figure 3C combines the marginal plots of figures 3A and 3B, plotting effect size against mean correlation with each simulation as a single dot. The color of the dot indicates which of the four models had the highest  $R^2$  for that simulation. While this depiction ignores the margin of victory by which a model is best, it nonetheless offers a useful graphical summary of model performance. In all four covariate scenarios, the kriging models tend to perform best at very low effect sizes (the left edge of the plots). Random forest, and to a lesser extent, treeing tend to be best at very low mean correlation (the bottom edge of the plots). In between, treeing tends to dominate across a wide swath of the plots. This nicely illustrates the benefits of treeing—while it may not be the best model in all cases, it is the generally the best when both the mean structure and dependence structures are informative and competitive when only one is.

## 4.2 Space-Time Case Studies

We evaluated the space-time predictive performance of treeing using the same  $\text{PM}_{2.5}$  and ozone data used in section 3.2 for spatial case studies. To provide insight into the potential impact of time series length, we estimated predictive accuracy on increasingly long subsets of the data from

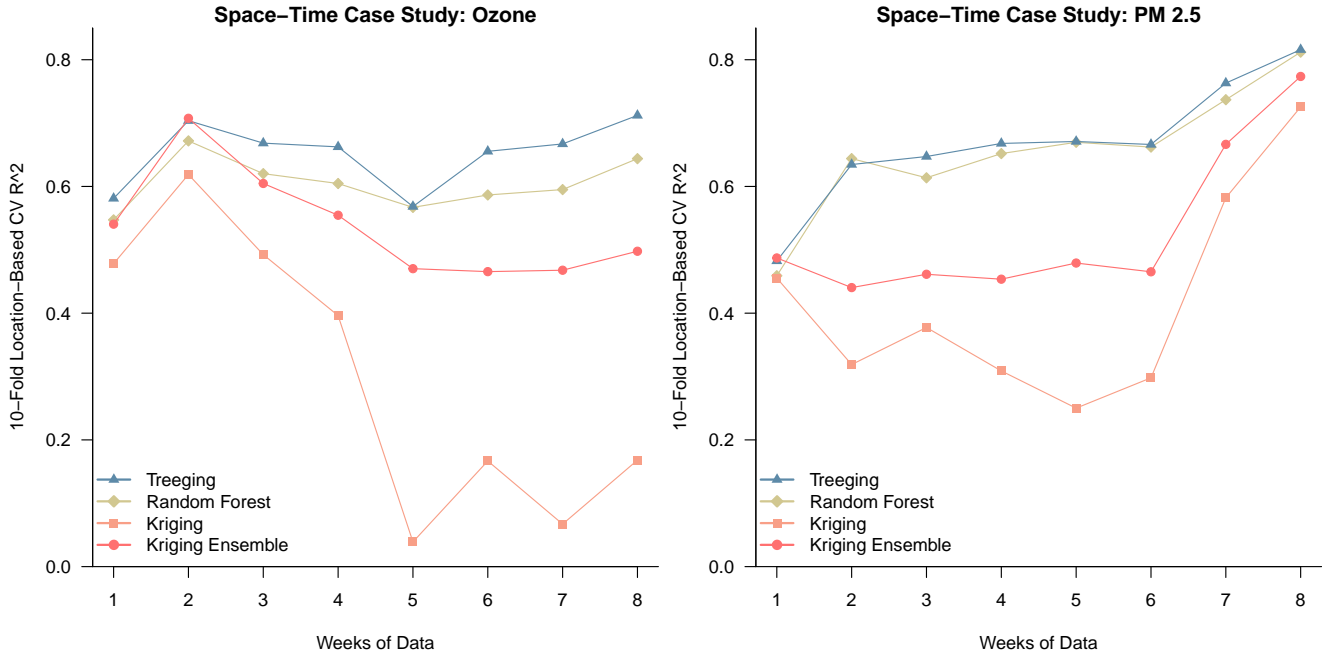


Figure 4: Space-Time Case Studies Model Comparison.

one to eight weeks. We used 10-fold location-based CV to estimate predictive accuracy in which the monitor locations were partitioned into 10 folds, so that all observations taken at a particular spatial location fall in the same fold. This is critical to avoid overly optimistic estimates of spatial interpolation prediction error (Watson et al., 2020b).

Figure 4 graphically depicts the  $\hat{R}_{CV}^2$  case study results. For both  $PM_{2.5}$  and ozone, treering is the best performing model, followed by random forest then ensembled kriging and lastly kriging. For  $PM_{2.5}$ , the difference in  $\hat{R}_{CV}^2$  between treering and random forest is very slight. For ozone, however, treering does provide a substantial improvement over random forest. This suggests that the covariates may be more informative for interpolating  $PM_{2.5}$ , similar to simulation scenario iii, while there may be informative covariates for ozone that are not contained in this data, as in simulation scenario iv.

The  $\hat{R}_{CV}^2$  for kriging and to a lesser extent ensembled kriging are both lower and more highly variable than treering and random forest in figure 4. The accuracy of kriging could potentially be improved with the use of a more sophisticated covariance estimation procedure. This may benefit kriging relative to random forest, but a more accurate covariance model would also benefit treering, which can use any covariance structure that kriging can. The greater variability of kriging

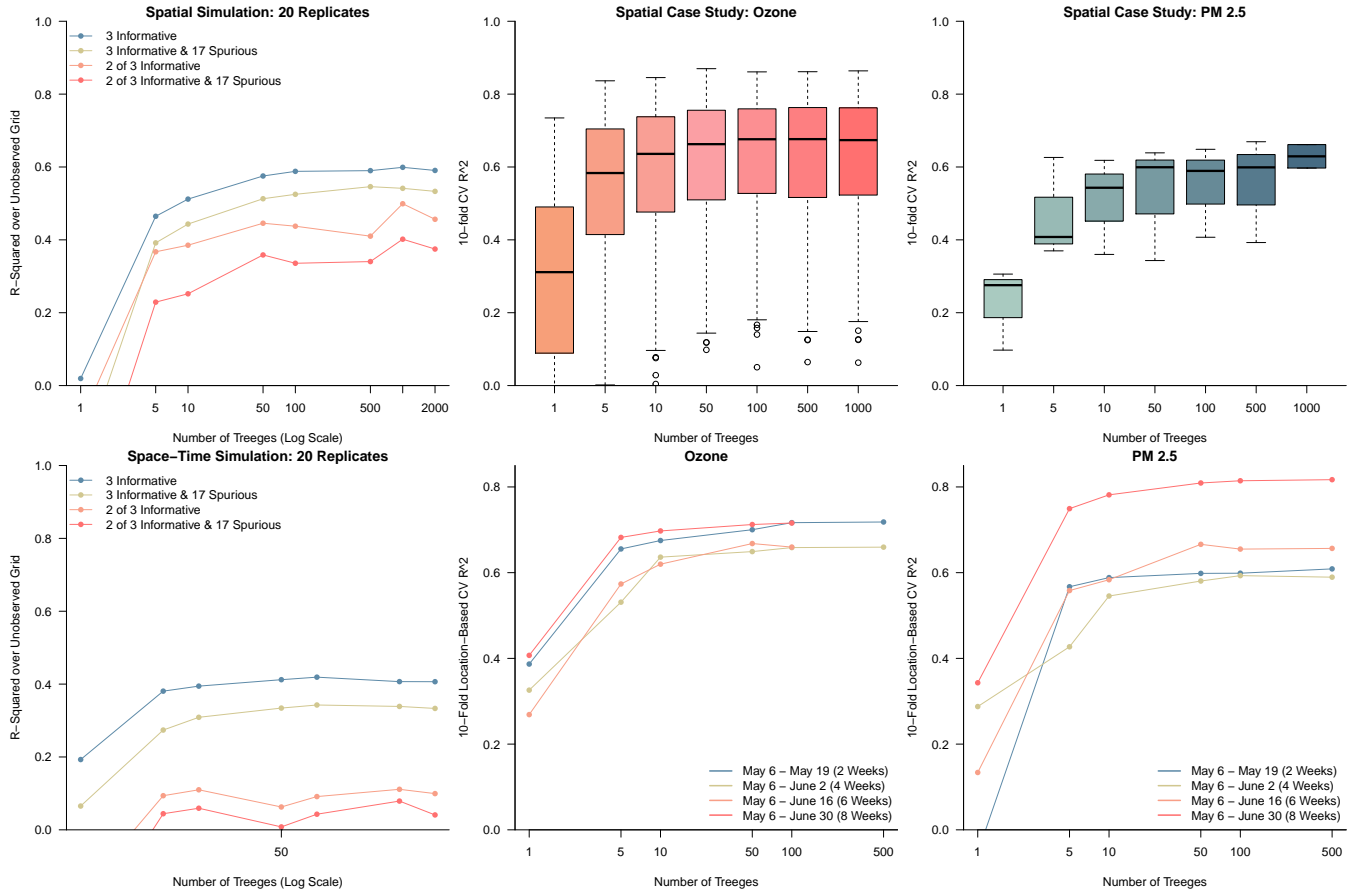


Figure 5: Tuning the Number of Treees

estimates reflects the potential for overfitting with a rigid mean structure that lacks a mechanism for feature selection. This is mitigated to some extent by the model averaging in the ensemble, but there is still greater variability than the tree-based ensembles.

## 5 Parameter Tuning

The two primary tunable parameters of treeing are the number of treees and the subsample proportion. Figures 5 and 6 depict predictive  $R^2$  (simulation) or  $\hat{R}_{CV}^2$  (case studies) for a variety of values of these parameters. In all cases, there is a substantial improvement in predictive accuracy from 1 to 5 treees, after which it generally increases until leveling off at 50 treees. In some cases there may be evidence of subsequent improvement, but based on these results we set 50 as the default number of treees. There is, of course, no guarantee this choice will be optimal



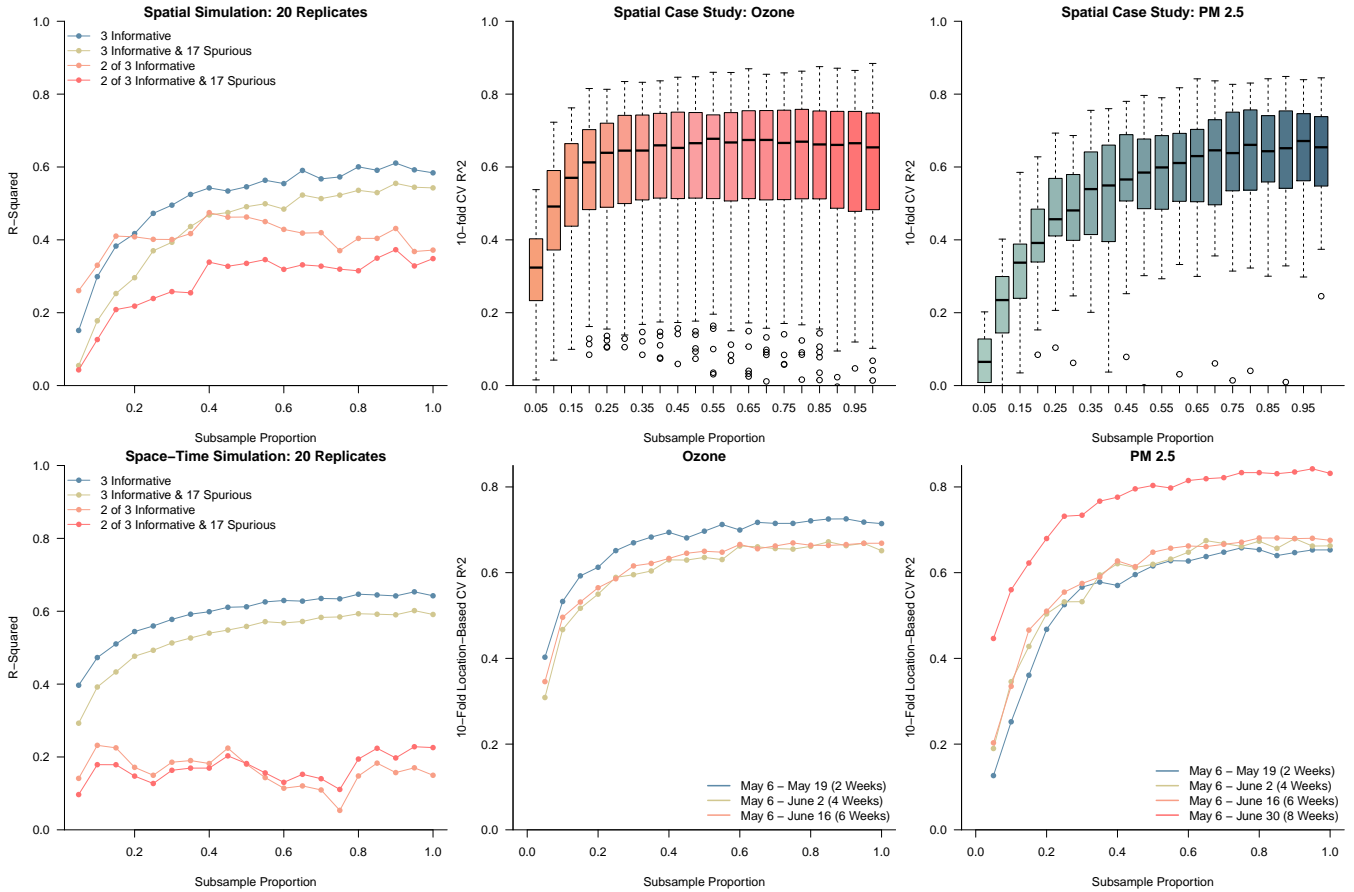


Figure 6: Tuning the Subsample Proportion

for a particular problem. Computing time increases with the number of trees, which may be an important consideration in the context of medium or large data.

Similarly, predictive accuracy increases initially with subsample proportion  $p$  and levels off. In both the spatial and space-time case studies, it seems to level off at a higher proportion for PM<sub>2.5</sub> than for ozone. In the spatial simulations there may be some evidence of an interesting divergence between scenarios in which all the informative covariates are observed (i and ii) and those in which an informative covariate is withheld (iii and iv). There appears to be a decrease in predictive accuracy for iii and iv for  $p > 0.75$ , whereas accuracy continues to increase for i and ii. It may be that higher subsample proportions can exacerbate the effects of overfitting when the covariates are misspecified. These results reinforce our default choice of  $p = 0.632$ , motivated by 0.632 being the expected proportion of the observations that appear in a bootstrap sample. There is a computational discount on the order of  $p^3$ , which again may be relevant for medium or

large data.

## 6 Large Data Set Approximations

Treeding is computationally intensive. However, it is feasible whenever kriging is. The computational complexity of kriging is  $o(n^3)$ , making each treege approximately  $o(p^3n^3)$  and a naive, sequential implementation of treeding  $o(Tp^3n^3)$ , where  $p$  is the subsample proportion and  $T$  is the number of treeges in the ensemble. Considerable gains can be made by parallelization, since treeges are fit independently.

Additional gains can be made by exploiting sparsity in  $\mathbf{X}_\tau(\mathbf{d})$  and spherical covariance matrices. The treege design matrix  $\mathbf{X}_\tau(\mathbf{d})$  has one nonzero element per row, a 1 at the column corresponding to the leaf in which the covariates associated with that row reside. Consequently, only  $L$  of its  $nL$  entries are nonzero, where  $L$  is the number of leaves in the treege. The estimated covariance matrix  $\hat{\Sigma}$  also tends to be sparse when a spherical covariance model is used, because the spherical covariance function decreases to 0 at a finite distance. Multiplying sparse matrices is generally substantially faster than dense matrices. The treeding R package uses the sparse matrix multiplication routines of the Basic Linear Algebra Subprograms (BLAS) via the Rcpp package (Dongarra, 2002; Eddelbuettel et al., 2011).

Treeding can also take advantage of strategies that have been developed to improve the scalability of kriging or Bayesian Gaussian process regression, such as Nearest-Neighbor Gaussian Processes (Datta et al., 2016).

## 7 Discussion

Treeding is an effective, new tool for spatial and space-time prediction. By enriching the flexible mean structure of regression tree base learners with the covariance structures of Gaussian process prediction and ensembling them, it combines the strengths of the two major classes of space-time prediction algorithms. While it is not the optimal model in all scenarios, it is clearly the best performing overall, whereas kriging suffers when dependence is weak or the mean structure is misspecified and random forest suffers when the covariates are uninformative.

Treeding offers clear advantages over alternatives that often rely on assumptions of smoothness and structural encoding of covariate effects (Berrocal et al., 2010; Szpiro et al., 2010). These do not offer the black box benefits of ensembling strategies that automatically learn regression surfaces, requiring subject level knowledge on the number of basis functions and how to encode covariates. The generative adversarial networks that have recently been applied to spatial interpolation problems (Zhu et al., 2020; Manepalli et al., 2020; Watson et al., 2020a; Gao et al., 2020) similarly require some level of subject knowledge, with expected performance of deep learning networks depending on a large number of tuning structures.

Most other approaches for enriching tree-based ensembles for dependent data have limited their focus to the spatial case. Post-hoc kriging of random forest residuals attempts to correct the fit of a traditional random forest using spatial dependence, but does not incorporate dependence into the ensemble base learners (Fayad et al., 2016; Fox et al., 2020). Incorporating spatial distances between observations (Hengl et al., 2018) along with values of nearby observations (Sekulić et al., 2020) as features may incorporate spatial information into random forest but in a restrictive manner and may greatly increase the number of features in the random forest. Alternatively, fitting a spatially localized random forest (Georganos et al., 2021) allows for spatial heterogeneity but requires selecting weight and bandwidth parameters, which adds computational complexity and may not perform well in the presence of nonstationarity.

Treed Gaussian processes (TGP) (Gramacy and Lee, 2008) and RF-GLS (Saha et al., 2021) are more closely related. TGP is a Bayesian regression tree with a GP at each leaf. This provides a very flexible probability model, but practically does not scale even to small air pollution space-time data sets like the approximately 13,000 observation ozone case study considered here, and convergence of MCMC over the space of regression trees remains challenging. The ensemble-based model averaging of treeding may also be preferable to the Bayesian model averaging of TGP, since the latter assumes a single regression tree as the underlying mean structure. It is likely and the goal of future work to show that treeding approximates the MAP (maximum a posteriori) under a particular, restrictive version of TGP. RF-GLS is an extension of random forest into a GLS framework for spatial data, and Saha et al. (2021) provide some theoretical guarantees that may hold for treeding as well.

A number of extensions and improvements to treeding present themselves as useful avenues for

future work. Naive ensembling could be extended to include a formalized notion of additivity and a formal optimization strategy, motivated by the well-known successes of boosting including on space-time air pollution problems (Watson et al., 2019; Reid et al., 2015). Localized subsampling may provide a useful alternative for tree construction, particularly in the presence of training data sampling bias. Random forest variable importance metrics may provide insight into the contribution of particular covariates within a tree ensemble. One could also explore bootstrap strategies for uncertainty quantification and possibly investigate the role of out-of-bag (OOB) error as estimator of interpolation error. Some work in IID cases has been published making use of the OOB error for random forest uncertainty quantification (Zhang et al., 2019). Finally, one could consider different flexible models for the mean structure.

## 8 Supplementary Materials

**Appendix:** Supplemental details on simulations and models. (pdf)

## References

- Berrocal, V. J., Gelfand, A. E., and Holland, D. M. (2010). A spatio-temporal downscaler for output from numerical models. *Journal of Agricultural, Biological, and Environmental Statistics*, 15(2):176–197.
- Boisvert, J., Manchuk, J., and Deutsch, C. (2009). Kriging in the presence of locally varying anisotropy using non-euclidean distances. *Mathematical Geosciences*, 41(5):585–601.
- Breiman, L. (2001). Random forests. *Machine learning*, 45(1):5–32.
- Cressie, N. (2015). *Statistics for spatial data*. John Wiley & Sons.
- Cressie, N. and Wikle, C. K. (2015). *Statistics for spatio-temporal data*. John Wiley & Sons.
- Datta, A., Banerjee, S., Finley, A. O., and Gelfand, A. E. (2016). Hierarchical nearest-neighbor gaussian process models for large geostatistical datasets. *Journal of the American Statistical Association*, 111(514):800–812.

- Dongarra, J. (2002). Basic linear algebra subprograms technical forum standard. *International Journal of High Performance Applications and Supercomputing*, 16(2):119–141.
- Eddelbuettel, D., François, R., Allaire, J., Ushey, K., Kou, Q., Russel, N., Chambers, J., and Bates, D. (2011). Rcpp: Seamless r and c++ integration. *Journal of Statistical Software*, 40(8):1–18.
- Efron, B. and Tibshirani, R. (1997). Improvements on cross-validation: the 632+ bootstrap method. *Journal of the American Statistical Association*, 92(438):548–560.
- Fayad, I., Baghdadi, N., Bailly, J.-S., Barbier, N., Gond, V., Hérault, B., El Hajj, M., Fabre, F., and Perrin, J. (2016). Regional scale rain-forest height mapping using regression-kriging of spaceborne and airborne lidar data: Application on french guiana. *Remote Sensing*, 8(3):240.
- Fox, E. W., Ver Hoef, J. M., and Olsen, A. R. (2020). Comparing spatial regression to random forests for large environmental data sets. *PloS one*, 15(3):e0229509.
- Gao, Y., Liu, L., Zhang, C., Wang, X., and Ma, H. (2020). Si-agan: Spatial interpolation with attentional generative adversarial networks for environment monitoring. In *ECAI 2020*, pages 1786–1793. IOS Press.
- Gelfand, A. E., Diggle, P., Guttorp, P., and Fuentes, M. (2010). *Handbook of spatial statistics*. CRC press.
- Georganos, S., Grippa, T., Niang Gadiaga, A., Linard, C., Lennert, M., Vanhuysse, S., Mboga, N., Wolff, E., and Kalogirou, S. (2021). Geographical random forests: a spatial extension of the random forest algorithm to address spatial heterogeneity in remote sensing and population modelling. *Geocarto International*, 36(2):121–136.
- Goldberger, A. S. (1962). Best linear unbiased prediction in the generalized linear regression model. *Journal of the American Statistical Association*, 57(298):369–375.
- Gramacy, R. B. and Lee, H. K. H. (2008). Bayesian treed gaussian process models with an application to computer modeling. *Journal of the American Statistical Association*, 103(483):1119–1130.

- Hengl, T., Nussbaum, M., Wright, M. N., Heuvelink, G. B., and Gräler, B. (2018). Random forest as a generic framework for predictive modeling of spatial and spatio-temporal variables. *PeerJ*, 6:e5518.
- Krige, D. G. (1951). A statistical approach to some basic mine valuation problems on the witwatersrand. *Journal of the Southern African Institute of Mining and Metallurgy*, 52(6):119–139.
- Lloyd, C. D. (2010). *Local models for spatial analysis*. CRC press.
- Manepalli, A., Singh, A., Mudigonda, M., White, B., and Albert, A. (2020). Generalization properties of machine learning based weather model downscaling. In Rush, A., editor, *Proceedings of the International Conference on Learning Representations*, pages 1–8.
- Paciorek, C. J. and Schervish, M. J. (2006). Spatial modelling using a new class of nonstationary covariance functions. *Environmetrics: The official journal of the International Environmetrics Society*, 17(5):483–506.
- Reid, C. E., Jerrett, M., Petersen, M. L., Pfister, G. G., Morefield, P. E., Tager, I. B., Raffuse, S. M., and Balmes, J. R. (2015). Spatiotemporal prediction of fine particulate matter during the 2008 northern california wildfires using machine learning. *Environmental Science & Technology*, 49(6):3887–3896.
- Saha, A., Basu, S., and Datta, A. (2021). Random forests for spatially dependent data. *Journal of the American Statistical Association*, (just-accepted):1–46.
- Sang, H. and Huang, J. Z. (2012). A full scale approximation of covariance functions for large spatial data sets. *Journal of the Royal Statistical Society: Series B (Statistical Methodology)*, 74(1):111–132.
- Sekulić, A., Kilibarda, M., Heuvelink, G., Nikolić, M., and Bajat, B. (2020). Random forest spatial interpolation. *Remote Sensing*, 12(10):1687.
- Stein, M. L. (2005). Space–time covariance functions. *Journal of the American Statistical Association*, 100(469):310–321.

- Szpiro, A. A., Sampson, P. D., Sheppard, L., Lumley, T., Adar, S. D., and Kaufman, J. D. (2010). Predicting intra-urban variation in air pollution concentrations with complex spatio-temporal dependencies. *Environmetrics*, 21(6):606–631.
- Watson, C. D., Wang, C., Lynar, T., and Weldemariam, K. (2020a). Investigating two super-resolution methods for downscaling precipitation: Esrgan and car. *arXiv preprint arXiv:2012.01233*.
- Watson, G. L., Reid, C. E., Jerrett, M., and Telesca, D. (2020b). Prediction & model evaluation for space-time data. *arXiv preprint arXiv:2012.13867*.
- Watson, G. L., Telesca, D., Reid, C. E., Pfister, G. G., and Jerrett, M. (2019). Machine learning models accurately predict ozone exposure during wildfire events. *Environmental Pollution*, 254:112792.
- Xu, Y., Ho, H. C., Wong, M. S., Deng, C., Shi, Y., Chan, T.-C., and Knudby, A. (2018). Evaluation of machine learning techniques with multiple remote sensing datasets in estimating monthly concentrations of ground-level pm<sub>2.5</sub>. *Environmental Pollution*, 242:1417–1426.
- Zhang, H., Zimmerman, J., Nettleton, D., and Nordman, D. J. (2019). Random forest prediction intervals. *The American Statistician*.
- Zhu, D., Cheng, X., Zhang, F., Yao, X., Gao, Y., and Liu, Y. (2020). Spatial interpolation using conditional generative adversarial neural networks. *International Journal of Geographical Information Science*, 34(4):735–758.